Inorganic Chemistry

Forum Article

pubs.acs.org/IC

Two-Photon Fluorescent Probes for Metal Ions in Live Tissues

Avik Ranjan Sarkar,[†] Dong Eun Kang,[‡] Hwan Myung Kim,*[,†] and Bong Rae Cho*[,‡]

[†]Division of Energy Systems Research, Ajou University, Suwon 443-749, Korea

[‡]Department of Chemistry, Korea University, 1-Anamdong, Seoul 136-701, Korea

ABSTRACT: Two-photon microscopy (TPM) is a new imaging tool that can detect biological targets deep inside a live tissue. To faciltate the use of TPM in biomedical research, a variety of two-photon (TP) probes for specific applications are needed. In this Forum Article, we describe the design strategy, photophysical properties, and biological imaging applications of a selection of our recent studies in the development of TP probes for metal ions. Small-molecule TP turn-on probes, organelle-targeted probes, and multicolor emissive probes for dual-color imaging are briefly reviewed.

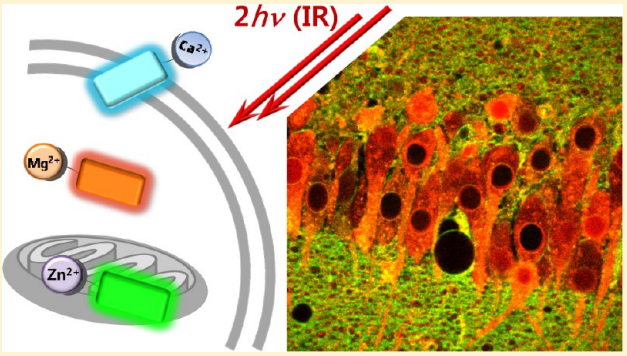

INTRODUCTION

One of the major subjects in inorganic chemistry is coordination chemistry studying the complexation of metal ions with various ligands. The metal-containing compounds are important in both inorganic chemistry and biology because they play key roles as structural or catalytic cofactors.[1,2] Free metal ions also play diverse roles in all cells of living organisms.[3] For proper cell function, the metal-ion homeostasis should be tightly controlled because disruption of their balance can cause aging and disease.[1−3] As such, understanding the roles of metal ions in a living system is an important research topic in bioinorganic chemistry.

To understand the roles of metal ions in biology, it is crucial to detect them in the live cell and tissue. Molecular imaging with fluorescent microscopy is a powerful tool for studying intracellular metal ions. In parallel, a large number of small-molecule probes, derived from common dyes such as fluorescein, BODIPY, rhodamine, and coumarin, and specific receptors for metal ions have been developed.[4,5] However, most of them have been developed for one-photon microscopy (OPM), which utilizes the fluorescence emitted from the probe-labeled cells for imaging. The excitation source of OPM is one UV−vis photon (λ_{ex} = 350−500 nm; Figure 1a). It has a shallow penetration depth (less than 100 μm) and can damage the cells and induce autofluorescence by exciting natural fluorophores such as nicotinamide adenine dinucleotide and flavin adenine dinucleotide.[6] As such, OPM is useful for cell imaging, not for long-term imaging of live tissues.[7]

An ideal tool to overcoming such limitations is two-photon microscopy (TPM).[8−10] TPM, which utilizes two near-infrared photons (λ_{ex} = 700−900 nm; Figure 1a) as the excitation source, is a new imaging tool that can visualize deep (more than 100 μm) inside a live tissue with minimum interference from self-absorption, autofluorescence, photodamage, and tissue preparation artifacts such as damaged cells that can extend

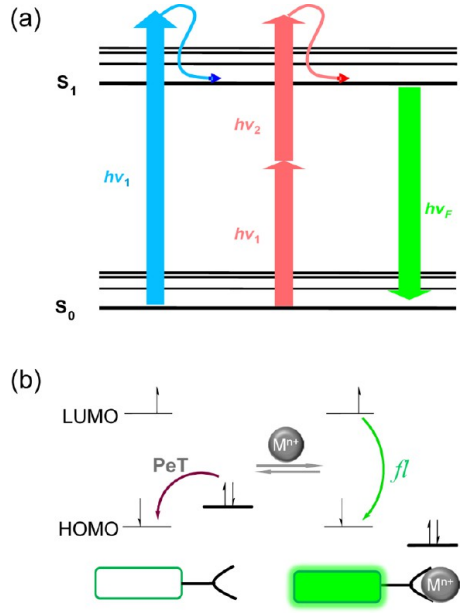

Figure 1. (a) Schematic diagram showing OP and TP excitation. The fluorescence is emitted from the S_1 state regardless of the excitation mode. (b) Molecular orbital diagram of a turn-on probe based on a PeT mechanism.

>70 μm into the tissue slice interior.[8−10] Because two-photon (TP) excitation is proportional to the square of the light intensity, TP excited fluorescence (TPEF) is emitted only at the focal point. This allows imaging of hundreds of $x-y$ planes

Special Issue: Imaging and Sensing

Received: May 28, 2013
Published: December 12, 2013

   dx.doi.org/10.1021/ic402475f | *Inorg. Chem.* 2014, 53, 1794−1803

along the z direction of a live tissue, from which a three-dimensional image can be constructed. However, the development of the TP probe was initiated less than 10 years ago, and there are a limited number of TP probes based on small organic molecules.[11−13] To expand the utility of TPM in bioimaging applications, there is a strong need to develop a variety of new TP probes that can detect specific cellular events deep inside an intact tissue with higher selectivity and sensitivity.

Recently, the design of new TP phosphorescent transition-metal complexes as biosensors and bioimaging reagents has become a rapidly emerging field.[14−17] While such complexes are useful for the sensing of oxygen by phosphorescence quenching,[14−16] they are not included in this paper because they have not yet been developed as a general method to detect metal ions in a living system.

In this Forum Article, we will briefly summarize the design strategy, photophysical properties, and biological imaging applications of a selection of TP probes for metal ions developed in our laboratories. We note that there are other recent reviews on related topics.[11−13] We will specifically focus on biologically essential metal ions, such as Zn^{2+}, Ca^{2+}, and Mg^{2+} ions.

DESIGN OF A TP PROBE FOR INTRACELLULAR METAL IONS

A first step toward designing effective TP probes requires consideration of the following criteria: (i) significant TP action cross section ($\Phi\delta_{TPA}$ > 50 GM), where Φ and δ_{TPA} are the fluorescence quantum yield and TP absorption (TPA) cross section, respectively, to obtain bright TPM images at low probe concentration and low laser power, (ii) high selectivity for target metal ions with appropriate dissociation constants (K_d), (iii) a large turn-on or ratiometric response of TPEF, (iv) appreciable water solubility for effective staining and cell permeability, and (v) high photostability for long-term imaging. These criteria are similar to those required for one-photon (OP) fluorescent probes except that TP probes require significant $\Phi\delta_{TPA}$ in place of the large Φ value required for OP fluorescent probes.

The TPA cross section is a function of the imaginary part (Imγ) of the second hyperpolarizbility (eq 1).[12]

$$\delta_{TPA}(\omega) \propto \mathrm{Im}[\gamma(-\omega;\ \omega,\ \omega,\ -\omega)] \qquad (1)$$

During the last 2 decades, extensive studies of the structure−property relationships have been undertaken to design a TP fluorophore having large δ_{TPA}.[18−20] The results of these studies have revealed that the magnitude of δ_{TPA} of electron donor−acceptor (D−A) dipoles, D−π−D and D−A−D quadrupoles, and two-dimensional octupoles increased with the extent of intramolecular charge transfer (ICT). Hence, the δ_{TPA} valued of such molecules can be increased by increasing the conjugation length and donor−acceptor strength. Because such a structural modification would inevitably increase the molecular weight (MW) and hamper biocompatibility, it is necessary to optimize MW and δ_{TPA} to obtain a suitable fluorophore for the TP probes. The water solubility can be increased by reducing the molecular size and introducing hydrogen-bonding sites, while the photostability can be increased by incoporating the conjugation bridge within the cycles. The TP fluorophores developed by considering these requirements are summarized in Chart 1. Compounds **1**−**5** were developed by us, while compond **6** was developed by Belfield et al.[21]

Chart 1. Structures of Typical TP Fluorophores for Small-Molecule TP Probes

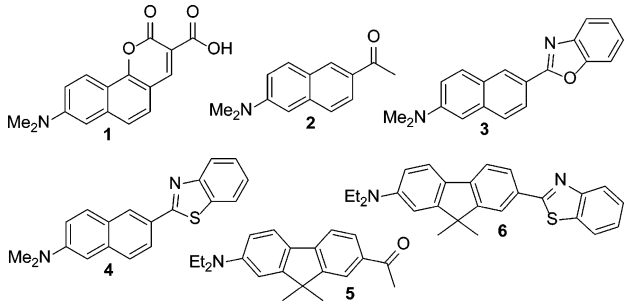

Selection of the metal-ion receptor is straightforward because numerous receptors for various metal ions are known in the literature.[22] Depending on how the receptors are linked to the fluorophores, two classes of TP probes can be designed.[23] One is a turn-on or turn-off probe, which undergoes changes in the TPEF intensity upon binding with metal ions. The other is a ratiometric probe, which responds with a chromic shift of the TPEF spectra during the binding events. Although ratiometric probes are useful for detecting metal ions quantitatively, they are rare, and most of the existing TP probes for metal ions are turn-on probes.

In recent years, we have developed a series of TP fluorescent turn-on probes derived from 8-(dimethylamino)-2-oxo-2*H*-benzo[*h*]chromene-3-carboxylic acid (chromene, **1**) and 2-acetyl-6-(dimethylamino)naphthalene (acedan, **2**) as the first generation TP probes for cytosolic metal ions.[13,24,25] More recently, organelle-targeted TP probes and probes for dual-color imaging for metal ions, derived from new TP fluorescent scaffolds including 6-(benzo[*d*]oxazol-2′-yl)-2-(*N*,*N*-dimethylamino)naphthalene (BODAN, **3**), 6-(benzo[*d*]-thiazol-2′-yl)-2-(*N*,*N*-dimethylamino)naphthalene (BTDAN, **4**), and 2-acetyl-7-(diethylamino)-9,9-dimethyl-9*H*-fluorene (AEMF, **5**), have been developed.[26−29] These probes were constructed by linking a receptor for the target metal ion to the TP reporter through a short spacer such as glycinamide.

We have employed planar TP fluorophores having a strong D−A pair to obtain significant δ_{TPA}. The sensing mechanism was based on a photoinduced electron-transfer (PeT) process;[23] that is, receptors with highest occupied molecular orbital (HOMO) levels higher than those of the fluorophores were used (Figure 1b). In the *apo* state, TPEF was quenched by PeT. Complexation with a metal ion lowered the receptor HOMO level, blocked PeT, and allowed TPEF emission. Small-molecule probes having hydrogen-bonding sites were developed to improve the water solubility and cell permeability while reducing the cytotoxicity. The specific examples are listed below, and their photophysical properties are summarized in Table 1.

TP FLUORESCENT PROBES FOR ZINC IONS

Zinc ion is an active component in enzymes and proteins.[30,31] The total zinc ion content in mammalian cells is approximately 0.2 mM, of which a small fraction exists as intracellular free Zn^{2+} ($[Zn^{2+}]_i$).[32] For proper cell functions, Zn^{2+} homeostasis must be tightly controlled because a low nanomolar concentration of free Zn^{2+} can be cytotoxic.[33] It is controlled by the import of $[Zn^{2+}]_i$ from and export to subcellular stores such as endoplasmic reticulum (ER) and mitochondria and to the extracellular space.[34] To visualize the $[Zn^{2+}]_i$ distribution

dx.doi.org/10.1021/ic402475f | Inorg. Chem. 2014, 53, 1794−1803

Table 1. Photophysical Properties of TP Probes in a Buffer

compound	solvent	$\lambda_{max}^{(1)}$ [a]	λ_{max}^{fl} [b]	Φ [c]	K_d^{OP}/ K_d^{TP} [d]	FEF [e]	$\lambda_{max}^{(2)}$ [f]	$\Phi\delta$ [g]
AZn1	H_2O [h]	365	496	0.02	1.10/1.10 nM	24.0	nd	nd
AZn1 + Zn^{2+}		365	498	0.47			780	86
AZn2	H_2O [h]	365	494	0.012	0.50/0.50 nM	52.0	nd	nd
AZn2 + Zn^{2+}		365	499	0.65			780	95
AZnM2	H_2O [i]	364	504	0.015	8.4/7.1 nM	4.0	nd	nd
AZnM2 + Zn^{2+}		363	504	0.42			780	110 [j]
AZnE2	H_2O [i]	366	503	0.026	23/21 nM	11.0	nd	nd
AZnE2 + Zn^{2+}		364	504	0.39			780	86
SZn-Mito	H_2O [k]	388	500	0.15	3.10/3.10 nM	7.0	nd	nd
SZn-Mito + Zn^{2+}		375	493	0.92			760	75 [l]
SZn2-Mito	H_2O [m]	413	536	0.0048	1.40/1.40 nM	68.0	nd	nd
SZn2-Mito + Zn^{2+}		395	536	0.33			750	155
ACa1	H_2O [n]	365	498	0.012	0.27/0.25 μM	44.0	nd	nd
ACa1 + Ca^{2+}		365	498	0.49			780	110
ACa2	H_2O [n]	362	495	0.010	0.14/0.16 μM	50.0	nd	nd
ACa2 + Ca^{2+}		362	495	0.42			780	90
ACa3	H_2O [n]	375	500	0.015	0.13/0.14 μM	23.0	nd	nd
ACa3 + Ca^{2+}		375	517	0.38			780	95
ACaL	H_2O [n]	369	500	0.0037	0.045 [o]/0.041 μM	10.0	nd	nd
ACaL + Ca^{2+}		372	502	0.43			780	90
ACaLN	H_2O [n]	364	498	0.0013	2.10/1.90 μM	13.0	nd	nd
ACaLN + Ca^{2+}		354	497	0.018			750	20
BCaM	H_2O [p]	360	470	0.07	90/89 μM [r]	14.0	nd	nd
BCaM + Ca^{2+}		360	470 [q]	0.98			780	150
FMg2	H_2O [s]	368	555	0.0058	1.40/1.70 mM	24.0	nd	nd
FMg2 + Mg^{2+}		368	555	0.12			740	76

[a] λ_{max} of the OP absorption spectra in nanometers. [b] λ_{max} of the OP emission spectra in nanometers. [c] Fluorescence quantum yield, ±15%. [d] Dissociation constants for Ni^{2+} in micromolars measured by OP (K_d^{OP}) and TP (K_d^{TP}) processes, ±8%. [e] Fluorescence enhancement factor, $(F - F_{mim})/F_{min}$. [f] λ_{max} of the TP excitation spectra in nanometers. [g] TP action cross section in 10^{-50} cm^4 s $photon^{-1}$ (GM). [h] 30 mM MOPS buffer (100 mM KCl, 10 mM EGTA, pH 7.2) in the absence and presence (1.8 μM) of free Zn^{2+}. [i] 30 mM MOPS buffer (100 mM KCl, 10 mM EGTA, pH 7.3) in the absence and presence (196 μM) of free Zn^{2+}. [j] 30 mM MOPS buffer (100 mM KCl, 10 mM EGTA, pH 7.3) in the absence and presence (1.3 μM) of free Zn^{2+}. [k] 30 mM MOPS buffer (100 mM KCl, 10 mM EGTA, pH 7.2) in the absence and presence (127 nM) of free Zn^{2+}. [l] 30 mM MOPS buffer (100 mM KCl, 10 mM EGTA, pH 7.2) in the presence (47 nM) of free Zn^{2+}. [m] 50 mM HEPES buffer (100 mM KCl, 10 mM NTA, pH 7.4) in the absence and presence (47 nM) of free Zn^{2+}. [n] 30 mM MOPS buffer (100 mM KCl, 10 mM EGTA, pH 7.2) in the absence and presence (39 μM) of free Ca^{2+}. [o] K_d^{OP} values measured in DPPC/CHL, DOPC, and a raft mixture are 0.082 ± 0.008, 0.11 ± 0.02, and 0.097 ± 0.010 μM, respectively. [p] 30 mM MOPS buffer (100 mM KCl, pH 7.2) in the absence and presence (2.5 mM) of free Ca^{2+}. [q] λ_{max}^{fl} values measured in LUVs composed of DPPC/CHL, a raft mixture, and DOPC are 436, 450, and 452 nm, respectively. [r] K_d values measured in LUVs and cells are 81 ± 4 and 78 ± 5 μM, respectively. [s] 30 mM MOPS buffer (100 mM KCl, 10 mM EGTA, pH 7.2) in the absence and presence (100 mM) of free Mg^{2+}.

inside live cells and living tissues, we have developed a series of TP probes for Zn^{2+} derived from acedan as the TP fluorophore and derivatives of *N*,N-di-(2-picolyl)ethylenediamine (DPEN) as the Zn^{2+} chelator (Chart 2). We adopted acedan from our earlier work on C-laurdan because it showed a $\Phi\delta_{TPA}$ value of 32 GM at 820 nm in water[35] and DPEN derivatives from the work of Nolan and Lippard.[36]

AZn1−AZnE2 are turn-on probes showing high selectivity and sensitivity for Zn^{2+}.[37,38] In a 3-(*N*-morpholino)-propanesulfonic acid (MOPS) buffer, the TPEF intensity of AZn2 increased gradually upon the addition of an increasing amount of Zn^{2+} (Figure 2a), a result observed by other probes. The K_d value of AZn2 calculated from the titration curve was 0.5 nM, which was suitable to detect intracellular free Zn^{2+} ($[Zn^{2+}]_i$). The K_d values of AZn1−AZnE2 are summarized in Table 1. The K_d value increased when a 2-Me substituent was introduced at the pyridyl moiety (AZn2 vs AZnM2) and as the spacer between the tertiary amino nitrogen and pyridyl moiety was lengthened (AZn2 vs AZnE2). For all receptors, the OMe group in the phenylene diamine moiety increased the TP fluorescence enhancement factors [$FEF^{TP} = (F - F_{min})/F_{min}$], while decreasing the dissociation constants (K_d^{TP}; Table 1). The OMe group seemed to elevate the HOMO of the receptor to facilitate PeT and decrease Φ of the *apo* state without affecting that of the probe−Zn^{2+} complex. It also increased the basicity of the receptor and enhanced the Zn^{2+} binding ability. AZn1−AZnE2 showed a $\Phi\delta_{TPA}$ value of ~90 GM at 780 nm in buffer solutions, a value ~4−24-fold larger than those of TSQ and FluZin-3 (Figure 2b and Table 1). This value allowed us to obtain much brighter TPM images of the cells labeled with these probes than those stained with commercially available probes.[37]

Chart 2. Structures of AZn1, AZn2, AZnM2, and AZnE2[37,38]

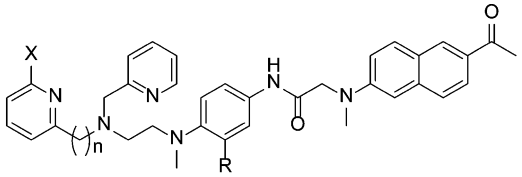

n = 1, X= H, R = H (**AZn1**); n = 1, X= H, R = OMe (**AZn2**);
n = 1, X= Me, R = OMe (**AZnM2**); n = 2, X= H, R = OMe (**AZnE2**)

dx.doi.org/10.1021/ic402475f | *Inorg. Chem.* 2014, 53, 1794−1803

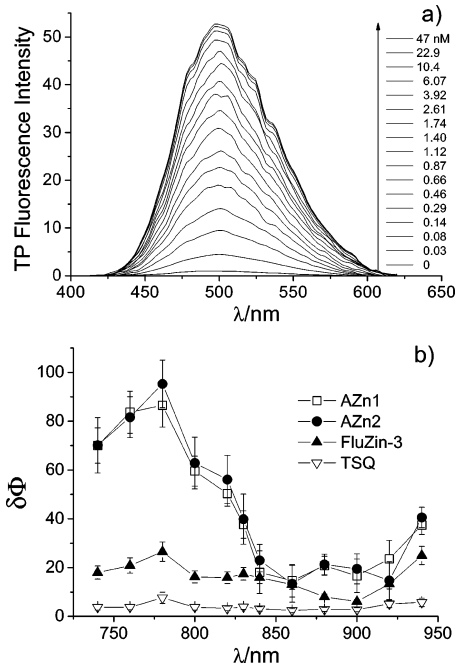

Figure 2. (a) TP fluorescence spectra of AZn2 in a MOPS buffer in the presence of free Zn^{2+} (0−47 nM). The excitation wavelength was 780 nm. (b) TP action spectra of AZn1 (□), AZn2 (●), FluZin-3 (▲), and TSQ (▽) in a MOPS buffer in the presence of 1.8 μM free Zn^{2+}. Reprinted with permission from ref 37. Copyright 2008 Wiley-VCH.

To test the utility of AZn1−AZnE2 in cell imaging, we obtained TPM images of the cells labeled with AZn1−AZnE2. The images were bright as expected from significant $\Phi\delta_{TPA}$ values. The TPM image of 293 cells labeled with AZn2 is shown in Figure 3 as a representative example. To confirm whether the bright regions reflected the $[Zn^{2+}]_i$ distribution, we monitored TPEF after treatment of the probe-labeled cells with *S*-nitrosocysteine (SNOC), a reagent that stimulates the cells to release Zn^{2+}, and *N*,*N*,*N*′,*N*′-tetrakis(2-pyridyl)ethylenediamine (TPEN), a membrane-permeable Zn^{2+} ion chelator that can effectively remove Zn^{2+} from the cells.[39] The TPEF intensity increased after the addition of SNOC and decreased upon treatment with TPEN (Figure 3). Similar results were observed with other probes. These results established that the bright regions were due to $[Zn^{2+}]_i$ and that AZn1−AZnE2 can detect $[Zn^{2+}]_i$ in live cells by TPM.

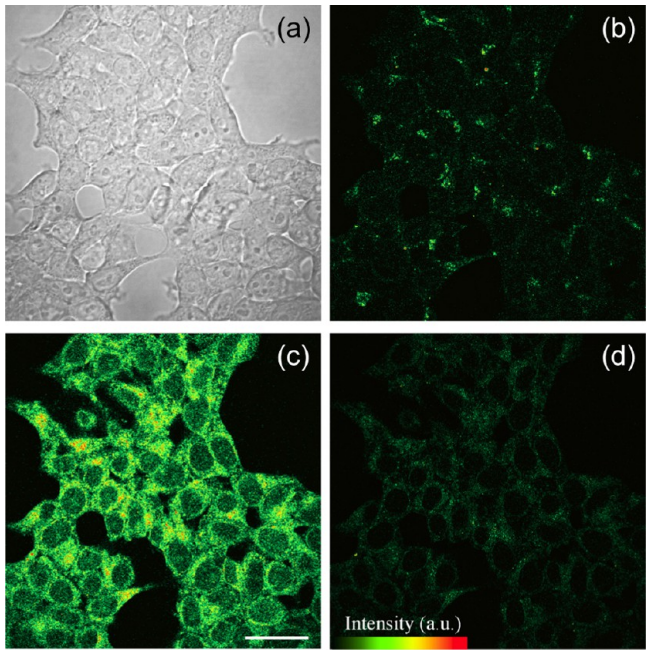

Figure 3. (a) Bright-field image. TPM images of AZn2-labeled 293 cells before (b) and after (c) the addition of SNOC to the imaging solution and (d) after the addition of TPEN to part c. Reprinted with permission from ref 37. Copyright 2008 Wiley-VCH.

We next assessed the utility of AZn1−AZnE2 in tissue imaging. TPM images of a part of a fresh rat hippocampal slice labeled with AZn2 are shown as a representative example (Figure 4). The image revealed bright regions in the stratum lucidum (SL) of CA3 and the hilus (H) of the dentate gyrus (DG; Figure 4a−c).[40] The TPEF intensity increased upon treatment with KCl, a membrane depolarizer that causes the release of Zn^{2+} (Figure 4b,c), and decreased after the addition of TPEN (for additional details, see ref 37). These results confirmed that the bright regions are due to $[Zn^{2+}]_i$. Further, the image obtained at 100× magnification in the SL of CA3 regions showed that $[Zn^{2+}]_i$ is concentrated in the mossy fiber axon terminals of the pyramidal neurons (Figure 4b). These findings established that AZn2 can detect intracellular free Zn^{2+} at 80−150 μm depth in live tissues using TPM.

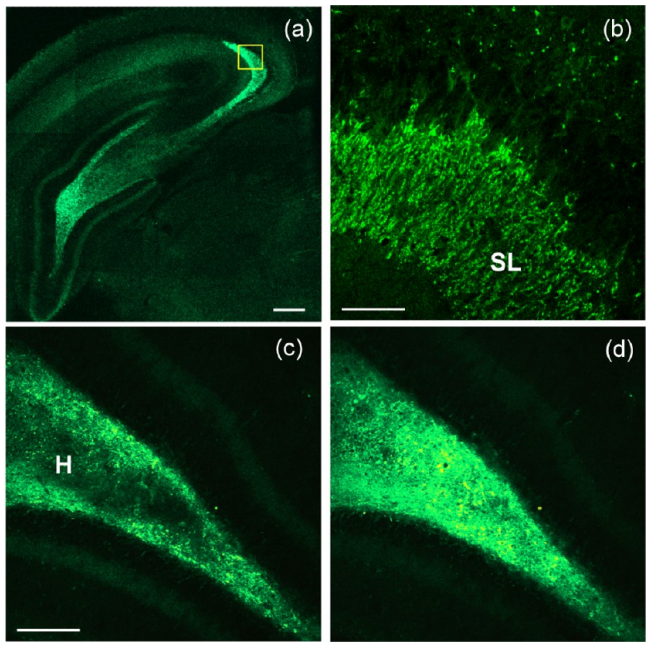

Figure 4. TPM images of a rat hippocampal slice stained with AZn2. (a) TPM image at a depth of ∼120 μm with magnification 10×. (b) Magnification at 100× in SL of CA3 regions (yellow box) at a depth of ∼100 μm. TPM images in H of DG regions at a depth of ∼100 μm (c) before and (d) after the addition of KCl to the imaging solution. Scale bars: (a and c) 300 and (b) 150 μm. Reprinted with permission from ref 37. Copyright 2008 Wiley-VCH.

■ MITOCHONDRIA-TARGETED TP PROBES FOR Zn^{2+}

Mitochondria are small organelles located in the cytoplasm that create energy for the cell's activity. They are the primary site for the consumption of oxygen and production of reactive oxygen species (ROS).[41,42] In mitochondria, zinc ions play important

dx.doi.org/10.1021/ic402475f | Inorg. Chem. 2014, 53, 1794−1803

roles as structural and catalytic cofactors.[43−46] While mitochondria can take up excess Zn^{2+} from cytoplasm to maintain Zn^{2+} homeostasis,[47,48] a strong elevation of intramitochondrial Zn^{2+} ($[Zn^{2+}]_{mito}$) can promote mitochondrial dysfunction.[47,48] To detect $[Zn^{2+}]_{mito}$, we have developed TP probes (SZn-Mito and SZn2-Mito, Chart 3) derived from

Chart 3. Structures of SZn-Mito and SZn2-Mito[26,27]

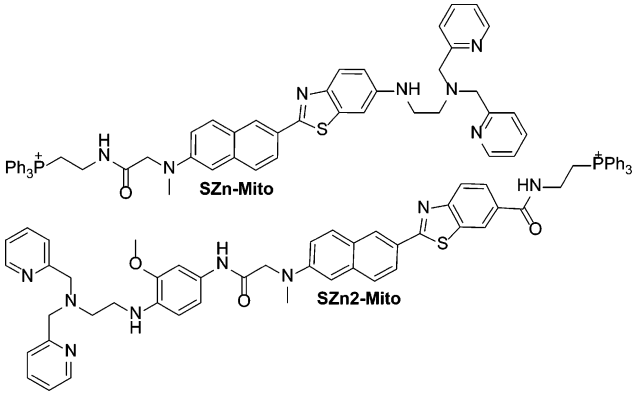

BTDAN as the reporter in conjunction with DPEN as the Zn^{2+} chelator[49] and triphenylphosphonium salt (TPP) as the mitochondrial targeting group.[50] TPP and DPEN were introduced at opposite ends of the probes to minimize the possible interactions between them (Chart 3).

SZn-Mito and SZn2-Mito are TP turn-on probes for $[Zn^{2+}]_{mito}$ showing FEF^{TP} values of 7 and 68 and K_d^{TP} values of 3.1 and 1.4 nM, respectively. The higher sensitivity and enhanced Zn^{2+} binding ability of SZn2-Mito having a 2-OMe group in the receptor moiety are consistent with those observed for AZn1−AZnE2 (Table 1). Both probes showed high selectivity for Zn^{2+}, significant $\Phi\delta$ values for the probe−Zn^{2+} complexes (75 and 155 GM), and pH insensitivity in the biologically relevant pH range. The larger $\Phi\delta$ value measured for the SZn2-Mito−Zn^{2+} complex was attributed to the amide moiety in the benzothiazole acceptor group that may have enhanced ICT. Thus, SZn2-Mito can detect a lower concentration of $[Zn^{2+}]_{mito}$ with higher sensitivity and a two times as bright TPM image than SZn-Mito, with minimum interference from other competing metal ions and the pH.

To test the utility of SZn2-Mito in cell imaging, we obtained a TPM image of HeLa cells labeled with SZn2-Mito. The image was bright, as expected from $\Phi\delta$ = 155 GM for the probe−Zn^{2+} complex. To confirm whether the bright regions reflected the $[Zn^{2+}]_{mito}$ distribution, we performed a colocalization experiment with HeLa cells colabeled with SZn2-Mito and Mitotracker Red FM, a commercial OP fluorescent probe for mitochondria.[22] The TPM image of SZn2-Mito overlapped well with the OPM image of Mitotracker Red FM (Figure 5a−c). Pearson's colocalization coefficient, *A*, calculated with *Autoquant X2* software, of SZn2-Mito with Mitotracker Red FM was 0.85.[51] Moreover, the TPEF intensity increased abruptly upon treatment of the probe-labeled cells with 2,2′-dithiodipyridine (DTDP), a reagent that promotes the release of Zn^{2+} from Zn^{2+}-binding proteins[52] (Figure 5d−g), and decreased sharply upon the addition of carbonyl cyanide *m*-chlorophenylhydrazone (CCCP), a compound that promotes the release of intramitochondrial cations by collapsing the mitochondrial membrane potential (Figure 5f,g).[53] These results confirmed that SZn2-Mito can detect ($[Zn^{2+}]_{mito}$) in live cells.

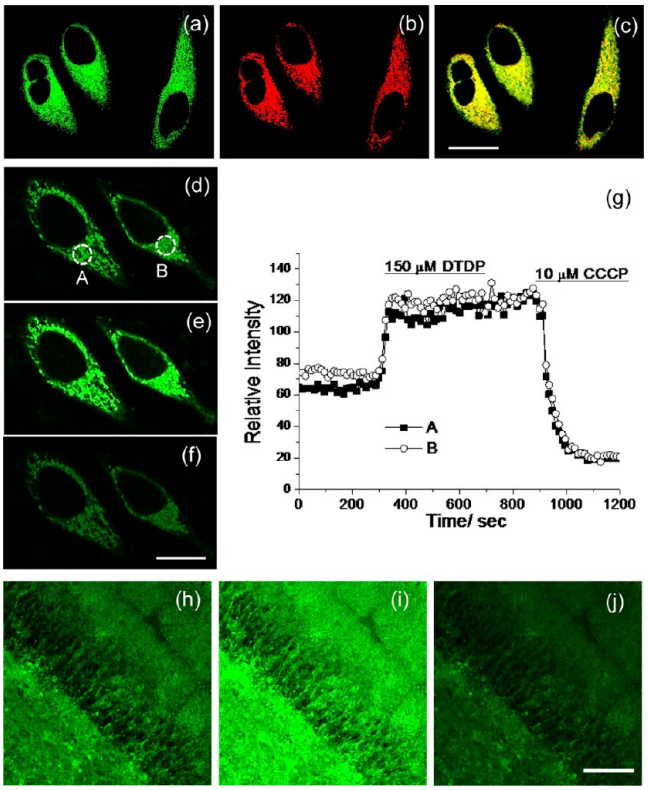

Figure 5. (a) TPM and (b) OPM images of HeLa cells colabeled with (a) SZn2-Mito and (b) Mitotracker Red FM. (c) Colocalized image. TPM images of SZn2-Mito-labeled HeLa cells, before (d) and after (e) the addition of 150 μM DTDP to the imaging solution and (f) after the addition of 10 μM CCCP to part e. (g) Relative TPEF intensity of SZn2-Mito-labeled HeLa cells as a function of time. TPM images at DG regions of a rat hippocampal slice stained with SZn2-Mito. Images were taken at a depth of ∼100 μm (h) before and (i) after the addition of 150 μM DTDP to the imaging solution and (j) after the addition of 10 μM CCCP to part i. Scale bars: (c) 20, (f) 10, and (j) 75 μm. Reprinted with permission from ref 26. Copyright 2012 Royal Society of Chemistry.

We then assessed the utility of SZn2-Mito in tissue imaging (Figure 5h−j). The TPM image of the probe-labeled tissue revealed bright regions in the DG at 100 μm depth.[26] At a higher magnification, the distribution of $[Zn^{2+}]_{mito}$ in the DG region was clearly visible (Figure 5h). To determine whether the bright regions reflected $[Zn^{2+}]_{mito}$, the probe-labeled tissue was treated with DTDP and CCCP. The TPEF intensity increased after the addition of DTDP and decreased upon treatment of CCCP, thereby confirming that the bright regions are due to $[Zn^{2+}]_{mito}$ (Figure 5h−j). These results established that SZn2-Mito can detect $[Zn^{2+}]_{mito}$ at 100 μm depth in a live tissue by using TPM.[26]

TP FLUORESCENT PROBES FOR CALCIUM IONS

Ca^{2+} is a ubiquitous intracellular messenger and plays a crucial role in physiology. Defective Ca^{2+} signaling is a feature of diverse diseases including hypertension and immunodeficiencies. The large transmembrane electrochemical Ca^{2+} gradient drives the entry of Ca^{2+} into cells.[54−56] Because cytosolic free Ca^{2+} ($[Ca^{2+}]_c$) must be kept low, the excess Ca^{2+} ions are extruded out of the cells.[54−56] Transport of Ca^{2+} across the cell membrane generates brief pulses of Ca^{2+}, which serves as a signaling system.[54−56] To understand the biological functions

dx.doi.org/10.1021/ic402475f | Inorg. Chem. 2014, 53, 1794−1803

of Ca^{2+}, it is important to visualize the Ca^{2+} activity in different cellular compartments such as the cytosol and at near-membrane locations.

We have developed a series of TP probes derived from acedan as the TP fluorophore and *O*,*O*′-bis(2-aminophenyl)-ethyleneglycol-*N*,*N*,*N*′,*N*′-tetraacetic acid (BAPTA) as the Ca^{2+}-selective chelator and visualized the calcium activities in the cytosol (ACa1−ACa3) and at near-membrane sites (ACaL and ACaLN) deep inside living tissues (Chart 4).[57−60]

Chart 4. Structures of ACa1−ACa3, ACaL, and ACaLN[57−60]

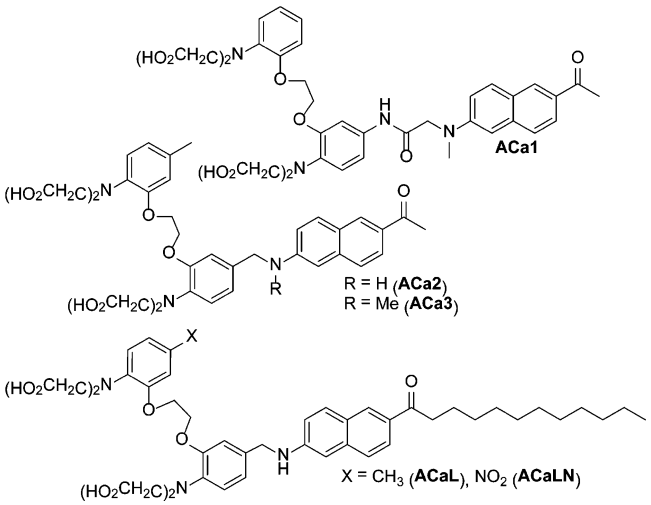

ACa1−ACa3 are TP turn-on probes with FEF^{TP} values of 23−50 and K_d^{TP} values of 0.14−0.25 μM, respectively (Table 1). The K_d^{TP} value changed significantly depending on the para substituents of BAPTA: the methyl group decreased K_d^{TP} from 0.25 to 0.16 μM (ACa1 vs ACa2), while the nitro group increased it from 0.041 to 1.90 (ACaL vs ACaLN), respectively (Table 1). ACa1−ACa3 showed high selectivity toward Ca^{2+} with the exception of Zn^{2+}, which is an intrinsic limitation of BAPTA, and pH insensitivity in the biologically relevant pH range. Moreover, $\Phi\delta_{max}$ values of the probe−Ca^{2+} complexes were 90−110 GM at 780 nm, respectively, which were larger than that of OG1−Ca^{2+} by 4-fold.[57,58] These results established that ACa1−ACa3 can detect intracellular free Ca^{2+} ions ($[Ca^{2+}]_i$), with a much brighter TPM image than those stained with OG1, in the regions where the chelatable Zn^{2+} concentration is much lower than the K_d^{TP} value of Ca^{2+}.

To test the utility of ACa1−ACa3 in cell imaging, we monitored the TPEF intensities in the astrocytes labeled with ACa1-AM. The TPM image revealed a spontaneous Ca^{2+} wave, which propagated from the astrocytic process to the soma and to the terminal (for additional details, see ref 58). The intercellular calcium wave was also observed, but it propagated at a slower rate. We then monitored the Ca^{2+} wave in fresh hypothalamic slices labeled with ACa2-AM. The spontaneous Ca^{2+} waves could be simultaneously visualized in the somata of neurons and astrocytes for more than 4000 s without appreciable decay (Figure 6). This outcome confirmed the utility of ACa2-AM in tissue imaging. In contrast, OPM images of the TTX-treated and fura-2-labeled thalamus slice[61] showed damaged cells on the tissue surface and were not as clear as the TPM images presented here. With fura-2, the fluorescence intensity showed appreciable decay after 500 s.[61] The use of ACa2-AM allowed improved TPM imaging in a probe-labeled

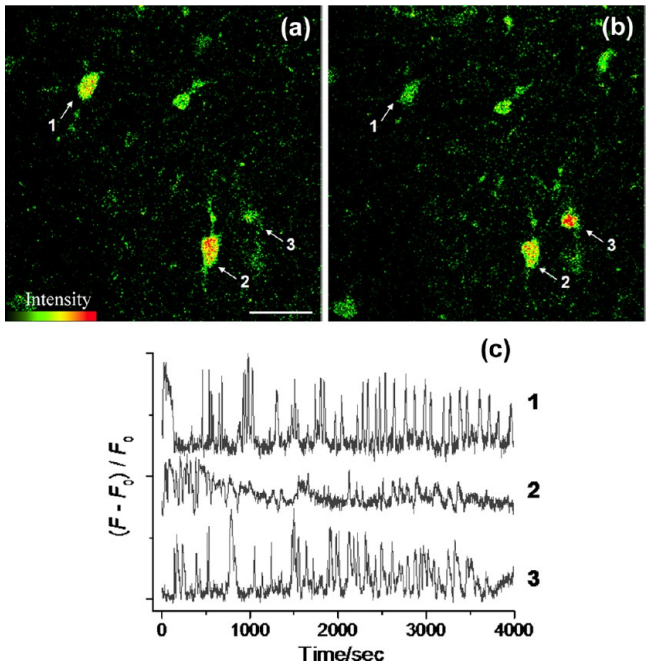

Figure 6. Pseudocolored TPM images of a fresh rat hypothalamic slice stained with ACa2-AM taken after 40 (a) and 1460 (b) s. Magnification at 100× shows a hypothalamic area at a depth of ~120 μm. (c) Spontaneous Ca^{2+} transients recorded in cells 1−3. Scale bar: 30 μm. Reprinted with permission from ref 58. Copyright 2008 Wiley-VCH.

live tissue at ~120 μm depth for a prolonged observation time. Furthermore, deep tissue images could be acquired with high photostability and low phototoxicity.

TP PROBES FOR NEAR-MEMBRANE CALCIUM IONS

To design TP probes for near-membrane Ca^{2+} ($[Ca^{2+}]_{mem}$), we considered two requirements. First, a receptor with a larger K_d value than BAPTA was used because the Ca^{2+} concentration was expected to be higher near the Ca^{2+} ion channels located in the plasma membrane than in the cytoplasm. Second, the probe was designed such that the Ca^{2+} receptor would be located near the lipid head groups of the plasma membrane and the hydrocarbon tail would be imbedded in the membrane interior. To meet such requirements, we employed the *p*-nitro derivative of BAPTA as the Ca^{2+} receptor and linked it to 2-(*N*-methylamino)-6-laurylnaphthalene (L) having a long-chain hydrocarbon tail through a short spacer (ACaL and ACaLN; Chart 4).[59,60]

ACaL and ACaLN are TP turn-on probes with FEF^{TP} values of 10 and 13,[59,60] and K_d^{TP} values of 0.041 and 1.9 μM, respectively. Both probes exhibited high selectivity toward Ca^{2+} and were pH-insensitive in the biologically relevant pH range. The $\Phi\delta_{max}$ values for ACaL and ACaLN in buffer solutions containing 39 μM Ca^{2+} were 90 (at 780 nm) and 20 GM (at 750 nm), respectively (Table 1). The $\Phi\delta_{max}$ value for ACaL was approximately 2.5-fold larger than that of Ca-green-Ca^{2+} and fura-2-Ca^{2+}, while the $\Phi\delta_{max}$ value of ACaLN was smaller than that of ACaL, which could be attributed to the smaller Φ value.[59,60]

To test the utility of ACaLN in cell imaging, we obtained a TPM image of clonal mouse hippocampal (HT22) cells labeled with ACaLN (Figure 7a). The image revealed bright domains

dx.doi.org/10.1021/ic402475f | Inorg. Chem. 2014, 53, 1794−1803

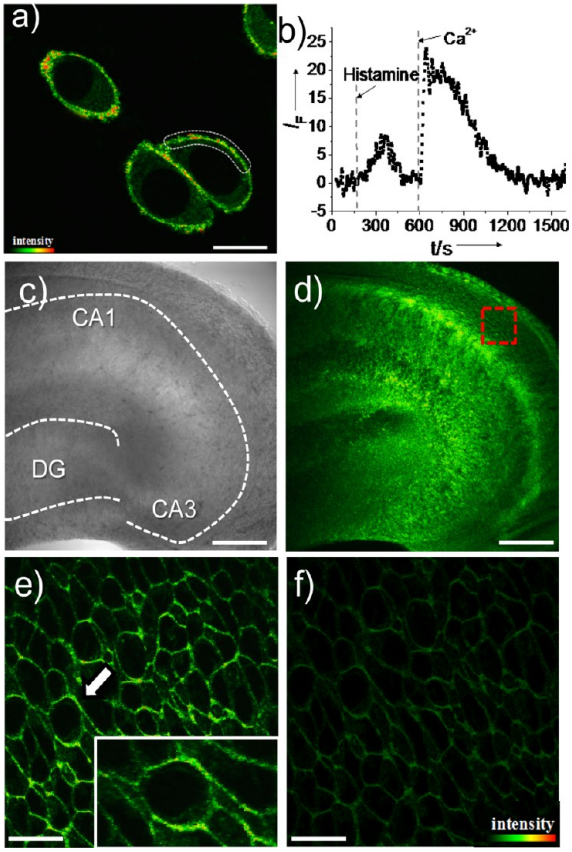

Figure 7. (a) Pseudocolored TPM images of HT22 cells labeled with ACaLN. (b) Time course of TPEF at the position marked with a dotted line in part a after stimulation with histamine in a nominally calcium-ion free buffer, followed by the addition of $CaCl_2$ to the imaging solution. Images of a fresh rat hippocampal slice labeled with ACaLN. (c) Bright-field images showing the CA1 and CA3 regions as well as DG upon 10× magnification. White dotted lines indicate the pyramidal neuron layers. (d) 10 TPM images collected in part c along the z direction at depths of 90−180 μm were accumulated. (e) TPM images of the red-labeled region at a depth of ∼120 μm by 100× magnification. (f) TPM images of the same region after the addition of EDTA to part e. The image in the white box is the enlarged image of the cells indicated by the white arrows. Scale bars: (a) 15, (e and f) 30, and (c and d) 300 μm. Reprinted with permission from ref 60. Copyright 2011 Wiley-VCH.

in the plasma membrane that could be attributed to the near-membrane Ca^{2+} (Figure 7a). We then monitored the TPEF intensities in the cell membrane after treatment of the probe-labeled cells with histamine, a reagent that stimulates the cells to release $[Ca^{2+}]_c$ from its intracellular reservoirs such as ER.[62,63] The TPEF intensity increased slowly after the addition of histamine, reaching a peak value after 150 s, apparently because it took some time for $[Ca^{2+}]_c$ to migrate to the cell membrane, and then decreased to the baseline intensity after 300 s (Figure 7b).[60] A similar result was observed with $CaCl_2$, except that the response was faster (Figure 7b). These results established that ACaLN can detect $[Ca^{2+}]_{mem}$ in a live cell.

We next evaluated the utility of ACaLN in tissue imaging. TPM images of a part of a fresh rat hippocampal slice incubated with ACaLN revealed the $[Ca^{2+}]_{mem}$ distribution in the CA1, DG, and CA3 regions. The image was brighter in CA1, indicating that $[Ca^{2+}]_{mem}$ is more abundant in CA1 than in the DG and CA3 regions (Figure 7d). At 100× magnification, the $[Ca^{2+}]_{mem}$ could be clearly visualized at a depth of 120 μm in a live tissue (Figure 7e). Further, the TPEF intensity decreased abruptly when the tissue was treated with ethylenediaminetetraacetic acid (EDTA; Figure 7f). These results confirmed that ACaLN can detect $[Ca^{2+}]_{mem}$ at 120 μm depth in a live tissue by TPM.

DUAL-COLOR IMAGING OF METAL-ION ACTIVITIES USING TP FLUORESCENT PROBES

Magnesium ion is the most abundant divalent metal ion in mammalian cells and is involved in many cellular processes, such as proliferation and cell death.[64−66] Calcium ion is another divalent metal cation that can regulate a variety of cellular functions.[54,56] The interactions between the two metal ions are important in certain biological processes. For example, Ca^{2+}/Mg^{2+} exchange is critical to the muscle contraction and relaxation.[67] Also, Mg^{2+} plays an active role in the Ca^{2+}-regulated cellular processes.[68,69] To understand such interactions in a living system, it is important to develop a tool to visualize Mg^{2+}/Ca^{2+} activities in a live tissue.[29]

To simultaneously visualize Mg^{2+}/Ca^{2+} activities, we have developed a pair of TP probes, BCaM and FMg2-AM, that emitted TPEF at 450 and 525 nm, respectively (Chart 5).

Chart 5. Structures of BCaM, FMg2, and FMg2-AM[28,29]

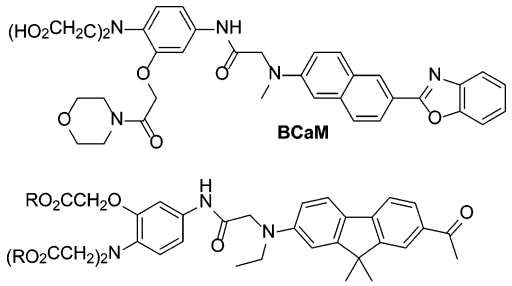

BCaM is a TP turn-on probe showing high sensitivity and selectivity for Ca^{2+} with $TPEF^{TP}$ of 14 and a K_d^{TP} value of 89 ± 3 μM, respectively. The K_d^{i} value, measured from digitonin-treated HeLa cells, of BCaM was 78 ± 5 μM, which was well within the range of $[Ca^{2+}]_{mem}$ in live cells (Table 1).[28] This probe showed a $\Phi\delta$ value of 150 GM at 780 nm in the presence of excess Ca^{2+} and pH insensitivity in the biologically relevant pH range and stained the cell membrane. Hence, BCaM was suitable to detect near-membrane Ca^{2+} ($[Ca^{2+}]_{mem}$) by TPM.

FMg2 was derived from AEMF (**5**) as the fluorophore[70] and *o*-aminophenol-*N*,*N*,*O*-triacetate as the Mg^{2+} receptor (Chart 5). It showed high sensitivity and selectivity for Mg^{2+} with FEF^{TP} = 24, K_d^{TP} = 1.7 ± 0.2 mM, and $\Phi\delta_{max}$ = 76 GM in the presence of excess Mg^{2+}, pH insensitivity in the biologically relevant range, high photostability, and low cytotoxicity, respectively.[29] Hence, FMg2 was suitable to detect cytosolic free Mg^{2+} ($[Mg^{2+}]_c$) by TPM.

To evaluate the utility of BCaM and FMg2-AM for dual-color cell imaging, we obtained a TPM image of the HepG2 cells colabeled with BCaM and FMg2-AM. Because TPEF spectra of the two probes were broad with emission maxima at 450 and 525 nm, respectively, we used 400−450 nm (Ch1 and BCaM) and 525−600 nm (Ch2 and FMg2-AM) as the detection windows.[29] The TPM images constructed from the

dx.doi.org/10.1021/ic402475f | Inorg. Chem. 2014, 53, 1794−1803

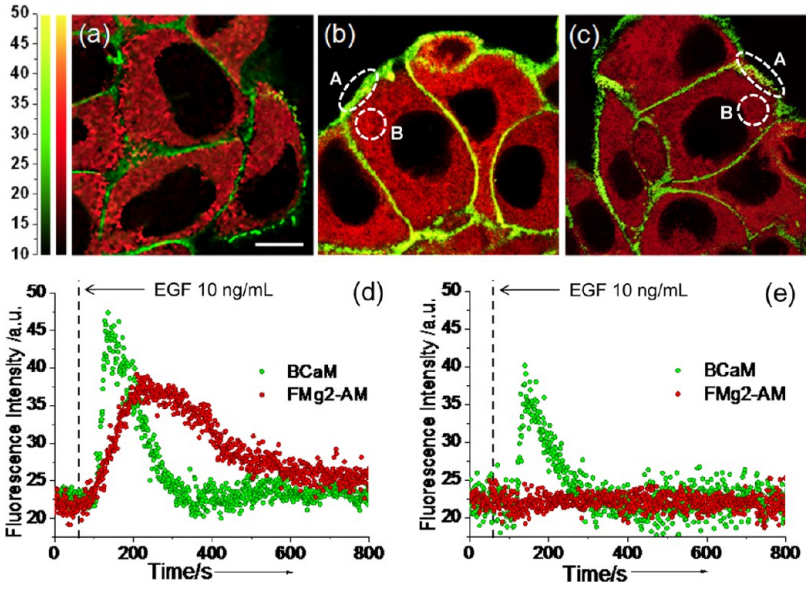

Figure 8. Dual-channel TPM images of HepG2 cells colabeled with BCaM and FMg2-AM collected at 400−450 nm (BCaM and Ch1) and 525−600 nm (FMg2-AM and Ch2), respectively. The TPM images were obtained in a PBS buffer (a), 200 s after stimulation with 5 μM calcimycin and 10 ng/mL EGF in the presence of 1.2 mM Mg^{2+} (b) or no Mg^{2+} (c). (d and e) Time course of TPEF at designated positions A (green curve) and B (red curve) in parts b and c, respectively, after stimulation. The TPEF intensities at A and B in parts b and c were measured before stimulation and normalized. Scale bar: 15 μm. Reprinted with permission from ref 29. Copyright 2012 American Chemical Society.

TPEF intensities clearly revealed green- and red-colored regions (Figure 8a−c).

To confirm whether the two regions reflected the distribution of $[Ca^{2+}]_{mem}$ and $[Mg^{2+}]_c$, we monitored the TPEF intensities at Ch1 and Ch2 after treatment of the probe-labeled cells with calcimycin, a Ca^{2+} ionophore that can allow Ca^{2+} to cross the cell membrane, and epidermal growth factor (EGF), a reagent that can induce a PLCγ1-dependent Ca^{2+} influx.[71] It is also known that the receptors that trigger Ca^{2+} influx through PLCγ1 can induce Mg^{2+} influx to regulate the Ca^{2+} influx.[69] When the two reagents were added to the probe-labeled cells in the presence of Mg^{2+}, the TPEF intensity increased sharply in the plasma membrane and then decreased to the baseline level (Figure 8d, green curve). A similar result was observed in the cytoplasm, albeit at a slower rate (Figure 8d, red curve). This outcome indicated that the EGF-induced transport of Ca^{2+} occurred at a faster rate than that of Mg^{2+}. We then conducted the same experiment in the absence of Mg^{2+}. Here again, the abrupt increase followed by the slow decrease in the TPEF intensity was observed, but to a lesser extent (Figure 8e, green curve). However, no change in the TPEF intensity was detected in the cytoplasm (Figure 8e, red curve). Depletion of Mg^{2+} reduced the EGF-induced influx rate of Ca^{2+} while nullifying that of Mg^{2+}.[29] These results established that FMg2 and BCaM can monitor Mg^{2+}/Ca^{2+} activities by dual-color imaging.

We next examined the utility of these probes in tissue imaging. We obtained 10 TPM images from Ch1 and Ch2 of a slice of a 14-day-old SD rat hippocampal tissue colabeled with BCaM and FMg2-AM at 100−200 μm depths (Figure 9b). The accumulated TPM images revealed $[Ca^{2+}]_{mem}$ and $[Mg^{2+}]_c$ distributions in the CA1, CA3, and DG regions (Figure 9b−e). The images collected at 100× magnification clearly revealed the distribution of $[Ca^{2+}]_{mem}$ and $[Mg^{2+}]_c$ in the pyramidal neuron layer composed of cell bodies in the CA1 region at a depth of 100 μm (Figure 9c,d). These results established that BCaM and FMg2 can simultaneously detect $[Ca^{2+}]_{mem}$ and $[Mg^{2+}]_c$ at 100−200 μm depth in live tissues by dual-channel TPM imaging.

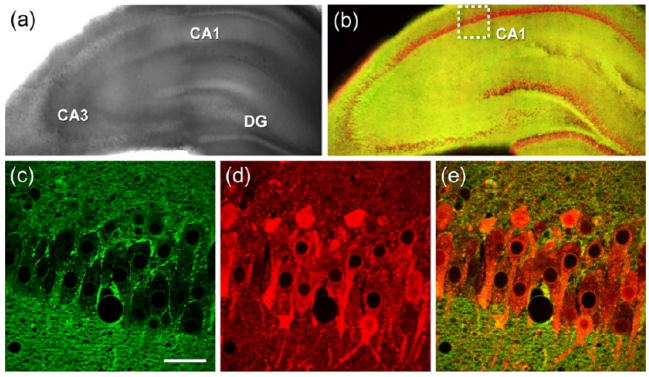

Figure 9. Images of a SD rat hippocampal slice colabeled with BCaM and FMg2-AM. (a) Bright-field images of the CA1-CA3 regions as well as DG at 10× magnification. (b) 10 TPM images collected at Ch1 and Ch2 (a) along the z direction at depths of approximately 100−200 μm were accumulated and then merged. (c−e) TPM images of CA1 regions collected at (c) Ch1 and (d) Ch2 at a depth of about 100 μm at 100× magnification. (e) Merged image of parts c and d. Scale bars: (b) 30 and (c) 300 μm. Reprinted with permission from ref 29. Copyright 2012 American Chemical Society.

CONCLUSIONS AND OUTLOOK

Because of its ability to provide molecular images deep inside intact tissues, TPM has become an important imaging tool for biomedical research. Indeed, a small-molecule TP-probe-based approach to TPM imaging in biological systems is a rapidly growing field that can significantly enhance the study of physiology and pathology.[72−78]

In this Forum Article, we have summarized a selection of our recent studies in small-molecule TP probes for metal ions including cytosolic turn-on probes, organelle targeted probes, and probes for dual-color imaging. All of them were developed

dx.doi.org/10.1021/ic402475f | Inorg. Chem. 2014, 53, 1794−1803

by linking the metal-ion receptors and organelle-specific functional groups to the TP fluorophores to meet all of the criteria outlined in the design of the TP probe section. The combination of a specific receptor and an efficient TP fluorophore through a short spacer has been a successful strategy for the design of TP turn-on probes for metal ions, which can be extended to many other analytes, organelle markers, and bioconjugates. Simultaneous detection of two metal ions in a live tissue was possible by using two TP probes that emitted TPEF at widely separated wavelength regions.

Future research in this field should be directed toward the development of new TP fluorophores exhibiting larger $\Phi\delta_{TPA}$ values to obtain brighter TPM images using lower laser power and lower probe concentration, without hampering water solubility, photostability, and cell viability. TP fluorophores that emit TPEF at a wide range of emission maxima are also needed to develop probes for multicolor imaging. To maximally utilize the new TP fluorophore in the TP probe development, new design strategies may be required. In view of the limited number of existing TP probes, a large number of small-molecule TP probes for metal ions, ROS, reactive nitrogen species, and redox mediators are needed to facilitate the use of TPM in biomedical research. TP probes for specific applications such as organelle-targeted probes, emission ratiometric probes for quantitative analysis, enzyme substrates, markers for specific diseases, and various bioconjugates should also be developed. For simultaneous detection of multiple targets, TP probes that can detect different targets while emitting TPEF at widely different wavelength ranges are required.

AUTHOR INFORMATION

Corresponding Authors

*E-mail: kimhm@ajou.ac.kr.
*E-mail: chobr@korea.ac.kr.

Notes

The authors declare no competing financial interest.

ACKNOWLEDGMENTS

National Research Foundation (NRF) Grants 2011-0028663 and 2012007850, Priority Research Centers Program through the NRF (Grants 2009-0093826 and 20120005860), funded by the Ministry of Education, ICT & Future Planning and Korea Healthcare Technology R&D Project, Ministry of Health & Welfare, Republic of Korea (Grant A111182), are acknowledged.

REFERENCES

(1) Lippard, S. J.; Berg, J. M. *Principle of Bioinorganic Chemistry*; University Science Books: Mill Valley, CA, 1994.
(2) Finney, L. A.; O'Halloran, T. V. *Science* **2003**, *300*, 931.
(3) Alberts, B.; Johnson, A.; Lewis, J.; Raff, M.; Roberts, K.; Walter, P. *Molecular Biology of the Cell*, 4th ed.; Taylor & Francis Group: New York, 2002.
(4) Domaille, D. W.; Que, E. L.; Chang, C. J. *Nat. Chem. Biol.* **2008**, *4*, 168.
(5) Que, E. L.; Domaille, D. W.; Chang, C. J. *Chem. Rev.* **2008**, *108*, 1517.
(6) Zipfel, W. R.; Williams, R. M.; Christie, R.; Nikitin, A. Y.; Hyman, B. T.; Webb, W. W. *Proc. Natl. Acad. Sci. U. S. A.* **2003**, *100*, 7075.
(7) Rudolf, R.; Mongillo, M.; Rizzuto, R.; Pozzan, T. *Nat. Rev. Mol. Cell Biol.* **2003**, *4*, 579.
(8) Zipfel, W. R.; Williams, R. M.; Webb, W. W. *Nat. Biotechnol.* **2003**, *21*, 1369.
(9) Helmchen, F.; Denk, W. *Nat. Methods* **2005**, *2*, 932.
(10) Williams, R. M.; Zipfel, W. R.; Webb, W. W. *Curr. Opin. Chem. Biol.* **2001**, *5*, 603.
(11) Kim, H. M.; Cho, B. R. *Chem.—Asian J.* **2011**, *6*, 58.
(12) Sumalekshmy, S.; Fahrni, C. J. *Chem. Mater.* **2011**, *23*, 483.
(13) Yao, S.; Belfield, K. D. *Eur. J. Org. Chem.* **2012**, 3199.
(14) Lecoq, J.; Parpaleix, A.; Roussakis, E.; Ducros, M.; Goulam Houssen, Y.; Vinogradov, S. A.; Charpak, S. *Nat. Med.* **2011**, *17*, 893.
(15) Parpaleix, A.; Goulam Houssen, Y.; Charpak, S. *Nat. Med.* **2013**, *19*, 241.
(16) Finikova, O. S.; Lebedev, A. Y.; Aprelev, A.; Troxler, T.; Gao, F.; Garnacho, C.; Muro, S.; Hochstrasser, R. M.; Vinogradov, S. A. *ChemPhysChem* **2008**, *9*, 1673.
(17) Finikova, O. S.; Troxler, T.; Senes, A.; DeGrado, W. F.; Hochstrasser, R. M.; Vinogradov, S. A. *J. Phys. Chem. A* **2007**, *111*, 6977.
(18) Kim, H. M.; Cho, B. R. *Chem. Commun.* **2009**, 153.
(19) He, G. S.; Tan, L. S.; Zheng, Q.; Prasad, P. N. *Chem. Rev.* **2008**, *108*, 1245.
(20) Pawlicki, M.; Collins, H. A.; Denning, R. G.; Anderson, H. L. *Angew. Chem., Int. Ed.* **2009**, *48*, 3244.
(21) Yao, S.; Schafer-Hales, K. J.; Belfield, K. D. *Org. Lett.* **2007**, *9*, 5645.
(22) *A Handbook—A Guide to Fluorescence Probes and Lebeling Technologies*, 10th ed.; Haugland, R. P., Ed.; Molecular Probes: Eugene, OR, 2005.
(23) deSilva, A. P.; Gunaratne, H. Q. N.; Gunnlaugsson, T.; Huxley, A. J. M.; McCoy, C. P.; Rademacher, J. T.; Rice, T. E. *Chem. Rev.* **1997**, *97*, 1515.
(24) Kim, H. M.; Cho, B. R. *Acc. Chem. Res.* **2009**, *42*, 863.
(25) Kim, H. M.; Yang, P. R.; Seo, M. S.; Yi, J. S.; Hong, J. H.; Jeon, S. J.; Ko, Y. G.; Lee, K. J.; Cho, B. R. *J. Org. Chem.* **2007**, *72*, 2088.
(26) Baek, N. Y.; Heo, C. H.; Lim, C. S.; Masanta, G.; Cho, B. R.; Kim, H. M. *Chem. Commun.* **2012**, *48*, 4546.
(27) Masanta, G.; Lim, C. S.; Kim, H. J.; Han, J. H.; Kim, H. M.; Cho, B. R. *J. Am. Chem. Soc.* **2011**, *133*, 5698.
(28) Kim, H. J.; Han, J. H.; Kim, M. K.; Lim, C. S.; Kim, H. M.; Cho, B. R. *Angew. Chem., Int. Ed.* **2010**, *49*, 6786.
(29) Dong, X.; Han, J. H.; Heo, C. H.; Kim, H. M.; Liu, Z.; Cho, B. R. *Anal. Chem.* **2012**, *84*, 8110.
(30) Vallee, B. L.; Falchuk, K. H. *Physiol. Rev.* **1993**, *73*, 79.
(31) Frederickson, C. J.; Koh, J.-H.; Bush, A. I. *Nat. Rev. Neurosci.* **2005**, *6*, 449.
(32) Outten, C. E.; O'Halloran, T. V. *Science* **2001**, *292*, 2488.
(33) Vinkenborg, Ja. L.; Nicolson, T. J.; Bellomo, E. A.; Koay, M. S.; Rutter, G. A.; Merkx, M. *Nat. Methods* **2009**, *6*, 737.
(34) Colvin, R. A.; Holmes, W. R.; Fontaine, C. P.; Maret, W. *Metallomics* **2010**, *2*, 306.
(35) Kim, H. M.; Choo, H. J.; Jung, S. Y.; Ko, Y. G.; Park, W. H.; Jeon, S. J.; Kim, C. H.; Joo, T.; Cho, B. R. *ChemBioChem* **2007**, *8*, 553.
(36) Nolan, E. M.; Lippard, S. J. *Acc. Chem. Res.* **2009**, *42*, 193.
(37) Kim, H. M.; Seo, M. S.; An, M. J.; Hong, J. H.; Tian, Y. S.; Choi, J. H.; Kwon, O.; Lee, K. J.; Cho, B. R. *Angew. Chem., Int. Ed.* **2008**, *47*, 5167.
(38) Danish, I. A.; Lim, C. S.; Tian, Y. S.; Han, J. H.; Kang, M. Y.; Cho, B. R. *Chem.—Asian J.* **2011**, *6*, 1234.
(39) Sensi, S. L.; Ton-That, D.; Sullivan, P. G.; Jonas, E. A.; Gee, K. R.; Kaczmarek, L. K.; Weiss, J. H. *Proc. Natl. Acad. Sci. U. S. A.* **2003**, *100*, 6157.
(40) Koh, J. Y.; Suh, S. W.; Gwag, B. J.; He, Y. Y.; Hsu, C. Y.; Choi, D. W. *Science* **1996**, *272*, 1013.
(41) Turrens, J. F. *J. Physiol.* **2003**, *552*, 335.
(42) Dickinson, B. C.; Chang, C. J. *Nat. Chem. Biol.* **2011**, *7*, 504.
(43) Wood, Z. A.; Schroder, E.; Harris, J. R.; Poole, L. B. *Trends Biochem. Sci.* **2003**, *28*, 32.
(44) Carmel, R., Jacobsen, D. W., Eds. *Homocysteine in Health and Disease*; Cambridge University Press: Cambridge, U.K., 2001.
(45) Dalton, T. P.; Shertzer, H. G.; Puga, A. *Annu. Rev. Pharmacol. Toxicol.* **1999**, *39*, 67.

(46) Mari, M.; Morales, A.; Colell, A.; Garcia-Ruiz, C.; Fernandez-Checa, J. C. *Antioxid. Redox Signaling* **2009**, *11*, 2685.
(47) Sensi, S. L.; Yin, H. Z.; Weis, J. H. *Eur. J. Neurosci.* **2000**, *12*, 3813.
(48) Sensi, S. L.; Paoletti, P.; Bush, A. I.; Sekler, I. *Nat. Rev. Neurosci.* **2009**, *10*, 780.
(49) Komatsu, K.; Kikuchi, K.; Kojima, H.; Urano, Y.; Nagano, T. *J. Am. Chem. Soc.* **2005**, *127*, 10197.
(50) Murphy, M. P.; Smith, R. A. *Annu. Rev. Pharmacol. Toxicol.* **2007**, *47*, 629.
(51) Emmerson, K.; Roehrig, K. *Comp. Biochem. Physiol., Part B: Biochem. Mol. Biol.* **1992**, *103*, 663.
(52) Aizenman, E.; Stout, A. K.; Hartnett, K. A.; Dineley, K. E.; McLaughlin, B.; Reynolds, I. J. *J. Neurochem.* **2000**, *75*, 1878.
(53) Caporale, T.; Ciavardelli, D.; Di Ilio, C.; Lanuti, P.; Drago, D.; Sensi, S. L. *Exp. Neurol.* **2009**, *218*, 228.
(54) Berridge, M. J.; Bootman, M. D.; Roderick, H. L. *Nat. Rev. Mol. Cell Biol.* **2003**, *4*, 517.
(55) Orrenius, S.; Zhivotovsky, B.; Nicotera, P. *Nat. Rev. Mol. Cell Biol.* **2003**, *4*, 552.
(56) Rizzuto, R.; Pozzan, T. *Physiol. Rev.* **2006**, *86*, 369.
(57) Kim, H. M.; Kim, B. R.; Hong, J. H.; Park, J. S.; Lee, K. J.; Cho, B. R. *Angew. Chem., Int. Ed.* **2007**, *46*, 7445.
(58) Kim, H. M.; Kim, B. R.; An, M. J.; Hong, J. H.; Lee, K. J.; Cho, B. R. *Chem.—Eur. J.* **2008**, *14*, 2075.
(59) Mohan, P. S.; Lim, C. S.; Tian, Y. S.; Roh, W. Y.; Lee, J. H.; Cho, B. R. *Chem. Commun.* **2009**, 5365.
(60) Lim, C. S.; Kang, M. Y.; Han, J. H.; Danish, I. A.; Cho, B. R. *Chem.—Asian J.* **2011**, *6*, 2028.
(61) Parri, H. R.; Gould, T. M.; Crunelli, V. *Nat. Neurosci.* **2001**, *4*, 803.
(62) Lin, S.; Fagan, K. A.; Li, K. X.; Shaul, P. W.; Cooper, D. M. F.; Rodman, D. M. *J. Biol. Chem.* **2000**, *275*, 17979.
(63) Nagai, T.; Yamada, S.; Tominaga, T.; Ichikawa, M.; Miyawaki, A. *Proc. Natl. Acad. Sci. U. S. A.* **2004**, *101*, 10554.
(64) *Magnesium and the Cell*; Brich, N. J., Ed.; Academic Press: San Diego, CA, 1993.
(65) Cowan, J. A. *Biometals* **2002**, *15*, 225.
(66) Yang, W.; Lee, J. Y.; Nowotny, M. *Mol. Cell* **2006**, *22*, 5.
(67) Finley, N.; Dvoretsky, A.; Rosevear, P. R. *J. Mol. Cell Cardiol.* **2000**, *32*, 1439.
(68) Grabarek, Z. *Biochim. Biophys. Acta* **2011**, *1813*, 913.
(69) Li, F.-Y.; Chaigne-Delalande, B.; Kanellopoulou, C.; Davis, J. C.; Matthews, H. F.; Douek, D. C.; Cohen, J. I.; Uzel, G.; Su, H. C.; Lenardo, M. J. *Nature* **2011**, *475*, 471.
(70) Kucherak, O. A.; Didier, P.; Mely, Y.; Klymchenko, A. S. *J. Phys. Chem. Lett.* **2010**, *1*, 616.
(71) Xie, Z.; Peng, J.; Pennypacker, S. D.; Chen, Y. *Biochem. Biophys. Res. Commun.* **2010**, *399*, 425.
(72) Dong, X.; Yang, Y.; Sun, J.; Liu, Z.; Liu, B. F. *Chem. Commun.* **2009**, 3883.
(73) Rao, A. S.; Kim, D.; Nam, H.; Jo, H.; Kim, K. H.; Ban, C.; Ahn, K. H. *Chem. Commun.* **2012**, *48*, 3206.
(74) Liu, F.; Wu, T.; Cao, J.; Cui, S.; Yang, Z.; Qiang, X.; Sun, S.; Song, F.; Fan, J.; Wang, J.; Peng, X. *Chem.—Eur. J.* **2012**, *19*, 1548.
(75) Li, L.; Shen, X.; Xu, Q. H.; Yao, S. Q. *Angew. Chem., Int. Ed.* **2012**, *52*, 424.
(76) Yue, X.; Yanez, C. O.; Yao, S.; Belfield, K. D. *J. Am. Chem. Soc.* **2013**, *135*, 2112.
(77) Heo, C. H.; Kim, K. H.; Kim, H. J.; Baik, S. H.; Song, H.; Kim, Y. S.; Lee, J.; Mook-jung, I.; Kim, H. M. *Chem. Commun.* **2013**, *49*, 1303.
(78) Bae, S. K.; Heo, C. H.; Choi, D. J.; Sen, D.; Joe, E. H.; Cho, B. R.; Kim, H. M. *J. Am. Chem. Soc.* **2013**, *135*, 9915.